The International Journal of Advanced Manufacturing Technology (2022) 119:7415–7427
https://doi.org/10.1007/s00170-022-08752-w

ORIGINAL ARTICLE

Analysis of thermal error model of ball screw feed system based on experimental data

Jiancheng Yang[1] · Changyou Li[1] · Mengtao Xu[1] · Yimin Zhang[2]

Received: 13 April 2021 / Accepted: 15 January 2022 / Published online: 25 January 2022

Abstract

In order to investigate the effect of thermal expansion on the ball screw feed system (BSFS) of a precision machine tool, theoretical modeling of and experimental study on thermally induced error are focused in this paper. A series of thermal experiments are conducted on the machine tool to measure the temperature of the main heat source and measuring points of BSFS. This study is to classify the main heat sources and discuss the impact on the ball screw feed system separately. By the experimental data of ball screw system, the thermal model of screw shaft in the axial direction is analyzed and verified. Based on the heat generation and transfer analysis of ball screw system, thermal expansion of screw shaft in the axial direction is modeled mathematically. In addition, by analyzing the effects of machining parameters such as rotational speed, preloads, and lead, we get the parameter influence of BSFS's temperature rising and thermal deformation. This work can help us reduce thermal deformation effectively and improve the precision of CNC machining.

Keywords Temperature · Ball screw feed system · Thermal model · Experimental data · Influence factors

1 Introduction

Machine tools and their components are sensitive to temperature change that could exert an influence on mechanical structure deformation thereby inducing thermal error of motion drive systems [1]. Studies have shown that, for high-speed and high-precision machine tools, processing and manufacturing errors caused by thermal deformation account for about 40% to 70% of the total manufacturing errors [2]. Therefore, the research of machine tool thermal error has become an important research direction.

Of all factors that contribute to the thermal error of a machine tool, thermal error of ball screw system plays a very important role [1]. In order to investigate the thermal error of the ball screw, the finite element models are frequently performed [3]. Week uses the finite element method-possibilities and limitations to compute the thermal of machine tools [4]. Xu et al. [5] used the finite element method to estimate the thermal error of the ball screw system and effectiveness of the air cooling system. Ming and Jiang [6] developed an integrated thermal model by the aid of the finite-element method to analyze the temperature distribution of a ball screw feed drive system, considering the thermal contact resistance between the bearing and its housing. Li et al. [7] provides a comprehensive error compensation method for the time-varying positioning error of machine tools based on simulation and experimental analysis. Oyanguren et al. [8] presents a numerical modelling strategy to predict the preload variation due to temperature increase using a thermo-mechanical 3D finite element method based model for double nut-ball screw drives. Huang et al. [9] studies further the relationship between thermal deformation and heat quantity through modeling the thermal deformations of stretching bar and bending beam using heat quantity as the independent variable, and the stretching model is verified based on finite element method. Li et al. [10] develops an adaptive real-time model for predicting the thermal characteristics of the ball screw drive system on line with a finite element method integrated with the Monte Carlo method. Nevertheless, few researchers focused on how to get the analytical solution of the thermal model through theoretical methods.

✉ Changyou Li
chyli@mail.neu.edu.cn

[1] School of Mechanical Engineering and Automation, Northeastern University, Shenyang 110819, China

[2] School of Energy and Power Engineering, Shenyang University of Chemical Technology, Shenyang 110142, China

A good thermal error model with high accuracy and robustness is the key factor for error compensation [11–15]. Lee et al. [16] presents a thermal error model using a fuzzy logic strategy, which does not require any complex procedure such as multiregression or information about the characteristics of the plant. But the error model parameters are only calculated mathematically. Ma et al. [17] proposes the predictive model for thermal contact conductance based on the micro morphology description of rough surfaces and the contact load distribution of solid joints. Then, the dynamic thermal-structure model of the ball screw feed drive system was established. Han et al. [18] presents a new approach for building an effective mathematic thermal error for machine tools which is capable of improving the accuracy of the machine tool effectively. Wu et al. [19] introduced a comprehensive multiple regression method to study the relationship between temperature variation and thermal error for a ball screw system. Wang et al. [20] proposed a compound error model for the geometric and thermal errors of a milling center based on Newton interpolation. Most of the work done above focused on studying the relationship between thermal error and the temperature of the key heat source. However, under changing thermal conditions, the temperature field of the ball screw is usually inconsistent with the temperature of the key heat source.

There are also some researchers who focus on the measurement of temperature changes during the operation of machine tools. Wu et al. [21] proposes a thermal error model based on the five key temperature points by using genetic algorithm-based back propagation neural network, which improves the accuracy and reduces computational cost for the prediction of thermal deformation in the turning center. Xu et al. [22, 23] introduced an improved ball screw feed drive thermal error compensation system. Based on this system, the stroke input was calculated and modified by the controller of control unit, and then the compensation was completed. Zhang et al. [24] presents different prediction models for positioning error of ball screw feed drive system based on the mounting condition. And the coefficients in the model are identified using the multiple linear regression method. Wei et al. [25] leads to the proposal of a comprehensive temperature-feature extraction method that uses feature extraction algorithm and weight optimization to construct linear temperature-sensitive points. Experimental facilities verified the feasibility of its proposal. Sun et al. [26] presented a precision testing method called seven-sensor configuration method to measure the thermal errors of a horizontal machining center with linear optical grating scale. Li et al. [27] tests the temperatures and positional deviations of the ball screw feed drive system and the linear motor feed drive system equipped with linear scales and analyzes the factors that affect the positioning error. Then, the temperatures and positioning coordinates were used as inputs to build the thermally induced positional deviation model of full closed-loop feed drive system.

In this paper, based on the thermal boundary obtained from the experiment, we get the analytical solution of the thermal model of the ball screw feed system. Based on the definition of thermal expansion, the axial thermal elongation of the ball screw is calculated, and the temperature of the ball screw at different positions is measured experimentally, and the correctness of the model is verified by comparison with theoretical data. Finally, the influence of system parameters on the temperature field of the ball screw feed system is discussed.

2 Thermal error model of BSFS

2.1 Heat generation and thermal boundary conditions

The generation of heat is the root cause of the temperature rise and thermal deformation of the ball screw feed system. When the BSFS produces thermal deformation, thermal errors occur, too. Before discussing the thermal expansion and deformation of the BSFS, it is assumed that the ball screw is a solid cylindrical rod, and the temperature distribution in the radial direction is uniform.

2.1.1 Main heat source and heat generation

When the BSFS is in the transmission work, the heat is generated from friction heat, and the friction heat is mainly caused by the friction between the ball and the raceway or groove during the working process of the bearing and nut. Therefore, the main heat sources include the front and rear bearings and nut pairs, and the heat generation principle diagram is shown in Fig. 1.

During the working of the ball screw, friction and heat are generated between the bearing balls and the inner and outer rings of the bearing. The friction loss of the bearing is almost entirely converted into heat inside the bearing, which causes the temperature of the bearing to rise. The calorific value of the bearing can be calculated by the following empirical formula [28]:

$$Q_b = 1.047 \times 10^{-4} n M_1 \tag{1}$$

where Q_b is the calorific value of the bearing; n is the speed of the ball screw; and M_1 is the total friction torque of the bearing.

The preload of the ball screw nut pair will cause friction and heat generation of the nut pair. During the movement of the nut pair on the ball screw, the ball, the nut, and the groove of the ball screw will rub against each other, producing frictional heat, and the heat will be transferred to the ball

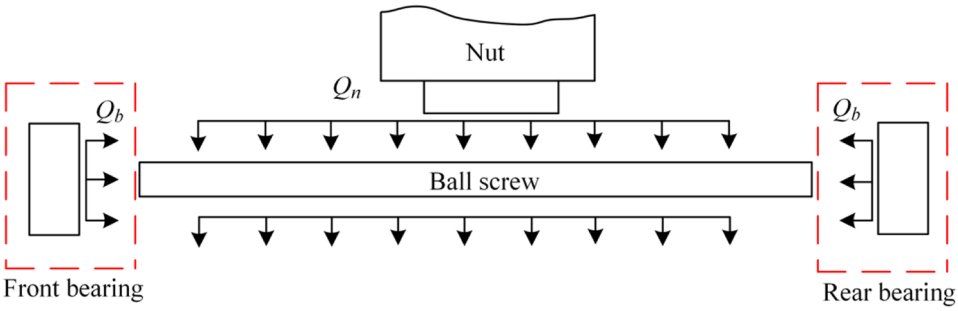

Fig. 1 Schematic diagram of heat generation of ball screw feed system

screw. It causes the temperature of the ball screw to rise. According to the empirical formula, the friction heat of the nut pair can be obtained by the following formula [29, 30]:

$$Q_n = 0.12\pi n f_0 \nu_0 M_2 \tag{2}$$

where Q_n is the calorific value of the nut; f_0 is the coefficient related to the nut type and lubrication method; ν_0 is the kinematic viscosity of the lubricating fluid; M_2 is the total friction torque of the nut.

According to the law of conservation of energy, it can be known that part of the heat generated by the bearing and nut is transferred to the screw, and the other part is lost to the air. The heat lost to the air includes two parts: heat convection heat dissipation and heat radiation heat dissipation. Since the heat radiation loss is relatively small, it can be ignored. Therefore, we have

$$\begin{cases} Q = Q_{sc} + Q_{sT} + Q_c \\ Q_{sc} = c_s m_s \left(T - T_0\right) \\ Q_{sT} = h_s A_s \left(T - T_0\right) \\ Q_c = h_c A_c \left(T_n - T_0\right) \end{cases} \tag{3}$$

where Q is the heat generated by the bearing or nut; Q_{sc} is the heat that causes the temperature of the ball screw to rise; Q_{sT} is the heat lost by the heat convection of the screw; and Q_c is the heat lost to the air by the nut heat convection. c_2 is the specific heat capacity of the ball screw; m_2 is the mass of the ball screw; h_c is the convective heat transfer coefficient of the nut; A_c is the surface area of the nut component; T_n is the temperature function of the nut; T_0 is the temperature of the air adjacent to the surface; A_s is the surface area of the ball screw; h_s is the convective heat transfer coefficient of the ball screw.

Heat dissipates from the ball screw shaft into the ambient air through forced convective heat transfer. The calculation of the heat transfer coefficient for convection follows a series of steps. First, the mean velocity of the fluid with respect to the solid surface is determined. When the parameter is known, the Reynolds number is determined. For the ball screw shaft rotating at an angular velocity of δ, the Reynolds number is written as

$$R_e = \frac{\delta d^2}{2\nu_l} \tag{4}$$

where ν_l is the kinematic viscosity of the air and d is the diameter of the screw shaft.

Second, the Nusselt number is determined by

$$N_u = 0.133 R_e^{2/3} P_r^{1/3} \tag{5}$$

where the Prandtl number P_r is a material parameter of the fluid and calculated as [31]

$$P_r = \frac{C_l \mu_l}{\gamma_l} \tag{6}$$

where C_l is the specific heat capacitance of the air, μ_l is the dynamic viscosity of the air, and γ_l is the thermal conductivity of the ambient air.

Then, the heat transfer coefficient is expressed as

$$h = \frac{N_u \gamma_l}{d} \tag{7}$$

2.2 Heat conduction equation of ball screw

The frictional heat of the bearing and the nut will cause the temperature rise of the ball screw, as its thermal behavior directly makes a great impact on the positioning error of the feed drive system. In order to obtain the thermal deformation of the ball screw, we established the heat conduction equation of the ball screw as follows [32]:

$$\frac{\partial^2 T(x,t)}{\partial x^2} = \frac{\rho c}{\lambda} \frac{\partial T(x,t)}{\partial t} \tag{8}$$

where λ is the thermal conductivity, ρ is the density, and c is the heat capacity.

At the start time, the initial temperature can be regarded as room temperature T_0. As for the heat boundary conditions of Eq. (8), there are mainly divided into two types [33]:

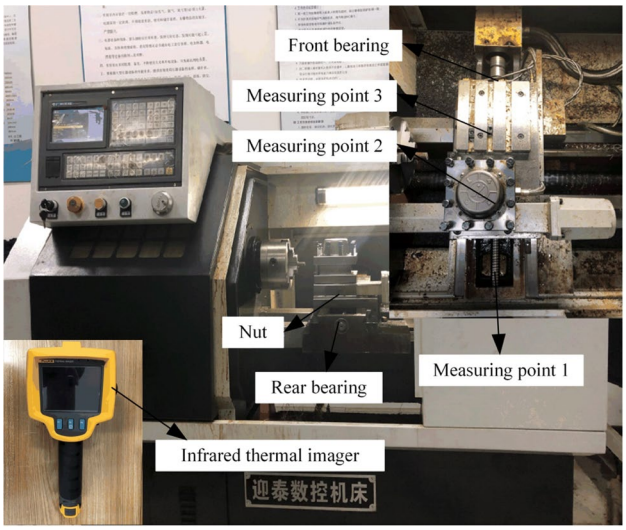

Fig. 2 CNC machine tool fittings

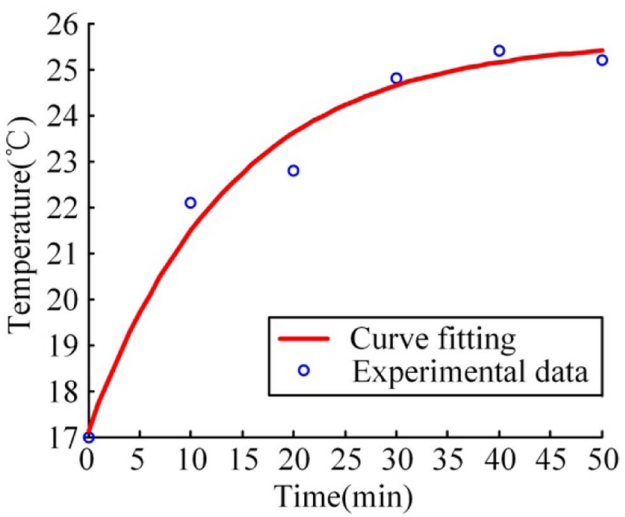

Fig. 3 The change curve of the temperature of the front bearing with time

i. At both ends of the screw shaft, it is supported by bearings, so the temperature at both ends is equal to the temperature of the bearing. Therefore, we have

$$T(x,t)|_{x=0,l} = T_b \tag{9}$$

where T_b is the bearing temperature; it can be obtained by polynomial fitting of experimental data.

ii. Assuming that the heat generated by the nut due to friction is uniformly applied to the ball screw [34], the temperature function of the nut can be obtained according to Eq. (3).

As shown in Fig. 1, three typical heat sources are contributing to the ball screw temperature rise. Because Eq. (8) is a linear differential equation, the temperature change of ball screw should be equal to the sum of temperature change responding to every single heat source. So we have

$$T(x,t) = \sum_{i=1}^{3} T_i(x,t) \tag{10}$$

2.2.1 Determination of boundary conditions

The test was completed on the Yingtai CJK6130 CNC machine tool, as shown in Fig. 2. Before the test, the ambient temperature T_0 was measured, and the measured initial ambient temperature was 17 °C. Then an infrared thermal imager is used to take pictures of the front and rear bearings and nut every 10 min during the working process of the machine tool, and the real-time temperature data are obtained as shown in Table 1.

The temperature curve of the bearing can be obtained by polynomial fitting as shown in Figs. 3 and 4. The temperature function of the bearing can be obtained in Eqs. (11) and (12):

$$T_{b1}(t) = 25.6303 - 8.506e^{-0.0718t} \tag{11}$$

$$T_{b2}(t) = 28.4766 - 11.3821e^{-0.0338t} \tag{12}$$

Similarly, the temperature curve of the nut bearing can be obtained by polynomial fitting, as shown in Fig. 5, and the temperature function of the nut can be obtained in Eq. (13):

$$T_n(t) = 30.6726 - 13.933e^{-0.0697t} \tag{13}$$

2.2.2 Solution of the heat conduction equation

Based on the experimental data, the temperature function of the boundary conditions is obtained by fitting. But the method of separating variables is only suitable for the case where the differential equations and boundary conditions

Table 1 Temperature of front and rear bearings and nut at different times

Time/min	0 min	10 min	20 min	30 min	40 min	50 min
Front bearing temperature/℃	17.0	21.1	22.7	24.8	25.6	25.2
Rear bearing temperature/℃	17.0	20.7	22.4	24.1	26.0	26.2
Nut temperature/℃	17.0	22.7	28.1	29.3	30.0	29.6

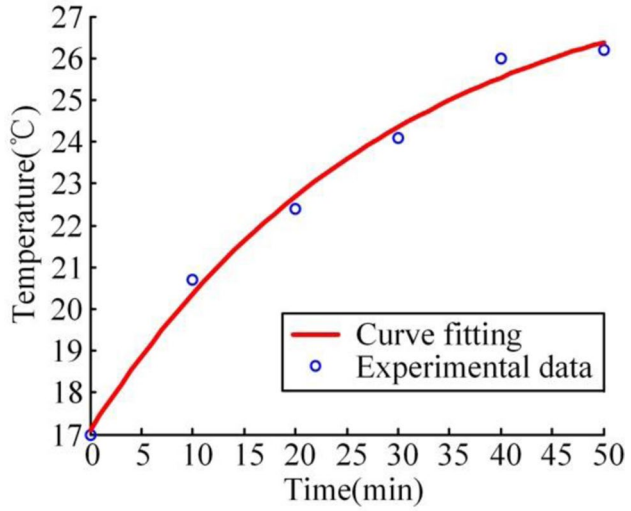

Fig. 4 The change curve of the temperature of the rear bearing with time

are both homogeneous, so we need to homogenize the non-homogeneous boundary conditions. The temperature function is expressed as the following form:

$$T(x,t) = u(x,t) + w(x,t) \tag{14}$$

where $w(x,t)$ is the selected known function and satisfies the Eqs. (11) and (12). The simplest selection method is the linear function of x as follows:

$$w(x,t) = A(t)x + B(t) \tag{15}$$

Substituting the boundary conditions into Eq. (15), the following equation can be obtained:

$$\begin{cases} A(t) = \frac{T_{b2}(t) - T_{b1}(t)}{L} \\ B(t) = T_{b1}(t) \end{cases} \tag{16}$$

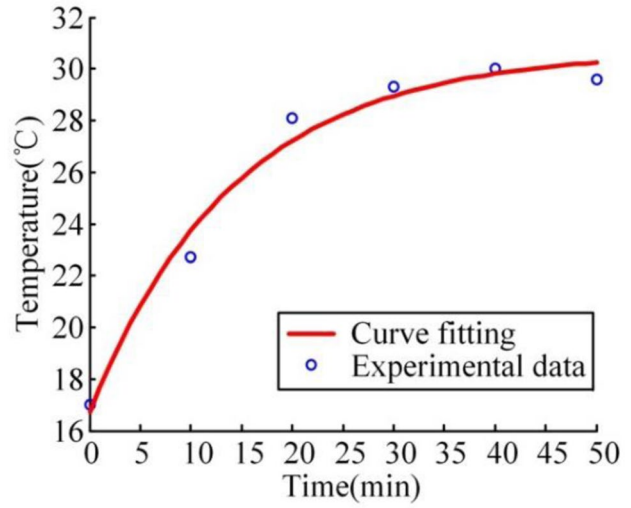

Fig. 5 The change curve of the temperature of the nut with time

where L is the length of the ball screw.

Substituting the Eq. (16) into the Eq. (15), so the $w(x,t)$ can be expressed as

$$w(x,t) = \frac{T_{b2}(t) - T_{b1}(t)}{L}x + T_{b1}(t) \tag{17}$$

Substituting Eqs. (14) and (15) into Eq. (8), the following equation can be obtained:

$$\frac{\partial^2 u(x,t)}{\partial x^2} - \frac{\partial u(x,t)}{\partial t} = \frac{\rho c}{\lambda}\frac{\partial w(x,t)}{\partial t} \tag{18}$$

As for Eq. (18), it is a non-homogeneous differential equation under homogeneous boundary conditions. So we need to solve the homogeneous analytical solution of the equation. We solve the homogeneous analytical solution of Eq. (19), and the Eq. (19) can be obtained as follows:

$$u(x,t) = u_1(x,t) + u_2(x,t) \tag{19}$$

where $u_1(x,t)$ is the solutions of homogeneous partial differential equations under homogeneous boundary conditions. $u_2(x,t)$ is the solutions of non-homogeneous partial differential equations under homogeneous boundary conditions.

$$\begin{cases} \frac{\partial^2 u_1(x,t)}{\partial x^2} - \frac{\partial u_1(x,t)}{\partial t} = 0 \\ u_1(0,t) = 0 \\ u_1(L,t) = 0 \\ u_1(x,0) = T_0 - w(x,0) \end{cases} \tag{20}$$

$$\begin{cases} \frac{\partial^2 u_2(x,t)}{\partial x^2} - \frac{\partial u_2(x,t)}{\partial t} = \frac{\rho c}{\lambda}\frac{\partial w(x,t)}{\partial t} \\ u_2(0,t) = 0 \\ u_2(L,t) = 0 \\ u_2(x,0) = 0 \end{cases} \tag{21}$$

First, we solve the relatively simple homogeneous partial differential equations. Suppose $u_1(x,t) = Y_1(x)\,F_1(t)$, then Eq. (20) can be expressed by the method of separating variables as follows [35]:

$$\frac{1}{Y_1(x)} \cdot \frac{d^2 Y_1(x)}{dx^2} = a\frac{1}{F_1(t)} \cdot \frac{dF_1(t)}{dt} \tag{22}$$

where a represents $\rho c/\lambda$.

If the above equation is true, then both sides must be equal to the same constant ($-\omega^2$); then the following equation can be obtained:

$$\frac{1}{Y_1(x)} \cdot \frac{d^2 Y_1(x)}{dx^2} = a\frac{1}{F_1(t)} \cdot \frac{dF_1(t)}{dt} = -\omega^2 \tag{23}$$

Therefore, we can get two differential equations from Eq. (23) as follows:

$$\begin{cases} \frac{d^2Y_1(x)}{dx^2} + \omega^2 Y_1(x) = 0 \\ a\frac{dF_1(t)}{dt} + \omega^2 F_1(t) = 0 \end{cases} \tag{24}$$

Solving the two differential equations in Eq. (24), then the solution result can be obtained:

$$\begin{cases} Y_r(x) = \sin\frac{r\pi}{L}x, r = 1, 2, 3... \\ F_1(t) = Ce^{-\frac{1}{a}\left(\frac{\pi r}{L}\right)^2 t} \end{cases} \tag{25}$$

where C is the integral constant, which can be obtained by the boundary conditions.

Therefore, substituting the Eq. (25) into $u_1(x,t) = Y_1(x)F_1(t)$, So the solution of $u_1(x,t)$ can be expressed as

$$u_1(x,t) = \sum_{r=1}^{\infty} Ce^{-\frac{\omega^2 t}{a}} \sin\frac{r\pi}{L}x, r = 1, 2, 3... \tag{26}$$

Then we solve the non-homogeneous partial equations under the homogeneous boundary by Fourier series expansion method [36]. Taking the solution of Eq. (20) as the eigenfunction which is $\sin(\pi rx/L)$, so the Fourier series of the result and the inhomogeneous term at the right end are expanded as follows:

$$u_2(x,t) = \sum_{r=1}^{\infty} q_r(t) \sin\frac{\pi r}{L}x \tag{27}$$

$$\begin{cases} f(x,t) = \sum_{r=1}^{\infty} f_r(t) \sin\frac{\pi r}{L}x \\ f_r(t) = \frac{2}{L}\int_0^L f(x,t) \sin\frac{\pi r}{L}x dx, r = 1, 2, 3... \end{cases} \tag{28}$$

Then substituting Eqs. (27) and (28) into Eq. (21), the following equation can be obtained:

$$\sum_{r=1}^{\infty}\left[-\left(\frac{\pi r}{L}\right)^2 q_r(t) \sin\frac{\pi r}{L}x\right] - \sum_{r=1}^{\infty} aq_r'(t) \sin\frac{\pi r}{L}x = \sum_{r=1}^{\infty} f_n(t) \sin\frac{\pi r}{L}x \tag{29}$$

By simplifying the Eq. (29), the following formula can be obtained:

$$q_r'(t) + \frac{\pi^2 r^2}{aL^2} q_r(t) - \frac{f_r(t)}{a} = 0, r = 1, 2, 3... \tag{30}$$

First, by solving the homogeneous solution of the differential equation corresponding to Eq. (30) and the Eq. (31), it can be obtained as follows:

$$q_r(t) = C_1 \cdot e^{-\frac{\pi^2 r^2}{aL^2} t} \tag{31}$$

Then we use the constant variation method to solve the special solution of Eq. (30). Supposed $C_1 = h(t)$, then Eq. (31) can be expressed as follows:

$$q_r(t) = h(t) \cdot e^{-\frac{\pi^2 r^2}{aL^2} t}, r = 1, 2, 3... \tag{32}$$

Substituting Eq. (32) and its derivative result into Eq. (32), the following formula can be obtained:

$$h'(t) \cdot e^{-\frac{\pi^2 r^2}{aL^2} t} - h(t) \cdot \frac{\pi^2 r^2}{aL^2} e^{-\frac{\pi^2 r^2}{aL^2} t} + h(t)\frac{\pi^2 r^2}{aL^2} e^{-\frac{\pi^2 r^2}{aL^2} t} - \frac{f_r(t)}{a} = 0, r = 1, 2, 3... \tag{33}$$

The solution results of $h(t)$ are as follows:

$$h(t) = \int \frac{f_r(t)}{a} e^{\frac{\pi^2 r^2}{aL^2} t} dt, r = 1, 2, 3... \tag{34}$$

So the solution of $q_r(t)$ can be obtained as follows:

$$q_r(t) = \left(\int \frac{f_r(t)}{a} e^{\frac{\pi^2 r^2}{aL^2} t} dt\right) \cdot e^{-\frac{\pi^2 r^2}{aL^2} t}, r = 1, 2, 3... \tag{35}$$

So the solution of the $u_2(x, t)$ can be obtained as follows:

$$u_2(x,t) = \sum_{r=1}^{\infty}\left(\int \frac{f_r(t)}{a} e^{\frac{\pi^2 r^2}{aL^2} t} dt\right) \cdot e^{-\frac{\pi^2 r^2}{aL^2} t} \cdot \sin\frac{\pi rx}{L} \tag{36}$$

Substituting Eqs. (17), (26) and (36) into Eq. (14), under considering the influence of bearing heat source, the temperature rise of the lead screw can be obtained:

$$T(x,t) = \left[\frac{T_{b2}(t) - T_{b1}(t)}{L}x + T_{b1}(t)\right] + \sum_{r=1}^{\infty}\left(C + \int \frac{\lambda f_r(t)}{\rho c} e^{\frac{\lambda}{\rho c}\frac{\pi^2 r^2}{L^2} t} dt\right) \cdot e^{-\frac{\lambda}{\rho c}\frac{\pi^2 r^2}{L^2} t} \cdot \sin\frac{r\pi x}{L} \tag{37}$$

Then, considering the influence of the uniform thermal boundary of the nut on the temperature rise of the ball screw, Eq. (13) is substituted into Eq. (3), and through the law of conservation of energy, Eq. (38) can be obtained as follows:

$$\frac{0.12\pi n L_b\left[F_a\left(1-\eta^2\right) + F_p(1-\eta)\right]t}{2\pi\eta} = \left(c_2 m_2 + h_s A_s t\right)\left(T - T_0\right)_t + h_c A_c\left(T_{nut} - T_0\right)t \tag{38}$$

After simplifying and separating Eq. (38), the temperature rise of the ball screw can be obtained:

$$\Delta T = \frac{0.12\pi n L_b\left[F_a\left(1-\eta^2\right) + F_p(1-\eta)\right] \times t/2\pi\eta - h_c A_c\left(T_{nut} - T_0\right)t}{c_2 m_2 + h_s A_s t} \tag{39}$$

where c_2 is the specific heat capacity of the ball screw; m_2 is the mass of the ball screw; h_c [37] is the convective heat

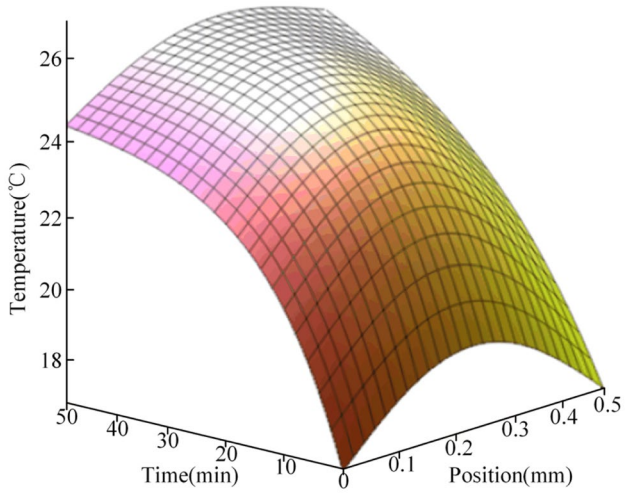

Fig. 6 The change curve of the temperature of the ball screw with time and position

transfer coefficient of the nut; A_c is the surface area of the nut assembly; F_p is the preload of the nut pair of the ball screw; L_b is the lead of the ball screw; η is the efficiency of the ball screw pair; F_a is the axial load; A_s is the surface area of the ball screw; and h_s is the convective heat transfer coefficient of the ball screw.

$$\Delta L = \int_0^L \alpha \left(\left[\frac{T_{b2}(t)-T_{b1}(t)}{L} x + T_{b1}(t) \right] + \sum_{r=1}^{\infty} \left(C + \int \frac{\lambda f_r(t)}{\rho c} e^{\frac{\lambda}{\rho c}\frac{\pi^2 r^2}{L^2} t} dt \right) \cdot e^{-\frac{\lambda}{\rho c}\frac{\pi^2 r^2}{L^2} t} \cdot \sin \frac{r\pi x}{L} + \frac{0.12\pi n L_b \left[F_a\left(1-\eta^2\right) + F_p(1-\eta) \right] \times t / 2\pi\eta - h_c A_c \left(T_{nut} - T_0 \right) t}{c_2 m_2 + h_s A_s t} - T_0 \right) dx \tag{43}$$

$$T(x,t) = \left[\frac{T_{b2}(t) - T_{b1}(t)}{L} x + T_{b1}(t) \right] + \sum_{r=1}^{\infty} \left(C + \int \frac{\lambda f_r(t)}{\rho c} e^{\frac{\lambda}{\rho c}\frac{\pi^2 r^2}{L^2} t} dt \right) \cdot e^{-\frac{\lambda}{\rho c}\frac{\pi^2 r^2}{L^2} t} \cdot \sin \frac{r\pi x}{L} + \frac{0.12\pi n L_b \left[F_a\left(1-\eta^2\right) + F_p(1-\eta) \right] \times t / 2\pi\eta - h_c A_c \left(T_{nut} - T_0 \right) t}{c_2 m_2 + h_s A_s t} \tag{40}$$

In summary, the temperature rise of the lead screw caused by the two types of heat sources is added together, and the temperature of the lead screw can be expressed as Eq. (40), and the change curve of the temperature of the ball screw with time and position is shown as Fig. 6.

2.3 Thermal deformation analysis

From a macro perspective, the thermal effect of the ball screw shaft of the ball screw feed system is axial elongation. For the screw shaft, the principle can be shown in Fig. 7.

Consider a very small part of ΔL_0 for analysis (ΔL_0 is small enough) (Fig. 8). At time t, the temperature increases from T_0 to $T(x, t)$, the length extends to $\Delta L(x)$, and the point x moves to x(t). The axial deformation at position x can be obtained by Eq. (41) [38]:

$$x(t) - x = \int_0^x \alpha \left(T(x,t) - T_0 \right) d\delta \tag{41}$$

where α is the thermal expansion coefficient.

So the thermal expansion deformation of a ball screw with a length of L can be expressed as

$$\Delta L = L(t) - L = \int_0^L \alpha \left(T(x,t) - T_0 \right) dx \tag{42}$$

Substituting Eq. (40) into Eq. (42), the following equation can be obtained:

3 Experimental verification of BSFS thermal error model

In the previous section, the temperature field model of the ball screw feed system has been established and solved analytically, and the temperature of the ball screw is obtained

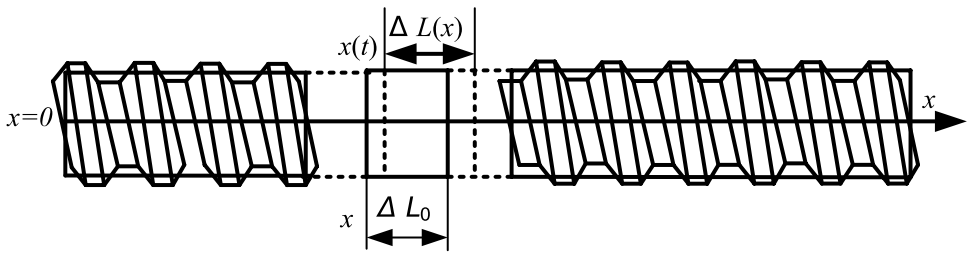

Fig. 7 Schematic diagram of thermal expansion analysis of ball screw

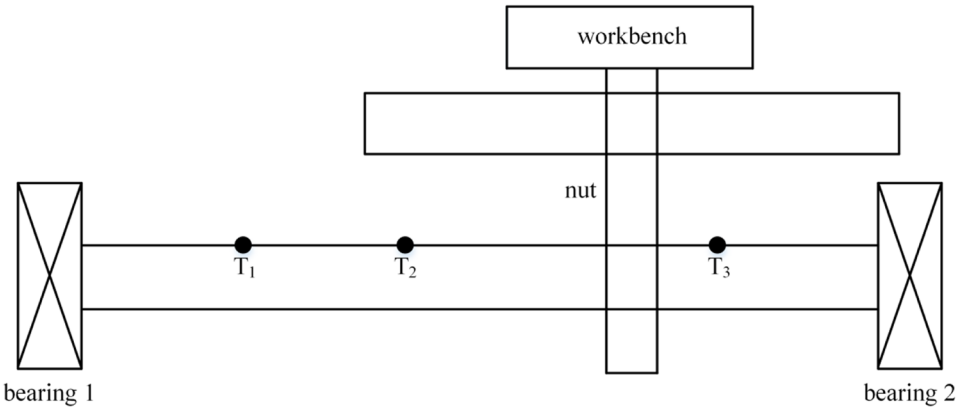

Fig. 8 Distribution of measured points for the ball screw

as a function of time and position. In order to verify the correctness of the model and the solution results, experiments are required verification. The correctness of the solution is verified by comparing the experimentally measured data with the theoretically calculated temperature. First, before the machine tool is started, measure the room temperature and record the initial temperature, and then select 3 points at 100 mm, 200 mm, and 400 mm on the lead screw as the test objects as shown in Figs. 2 and 7. Use an infrared thermal imager to measure the temperature of selected some points on the ball screw every 10 min and record it in Table 2.

Figure 9 shows the test measurement data at the 100-mm position of the ball screw and the theoretical simulation temperature versus time curve. Through calculation, it can be seen that the relative error between the test and the theoretical temperature is 10.38%, which is within the allowable tolerance within range.

Figure 10 shows the experimental measurement data at the 200-mm position of the ball screw and the theoretical simulation temperature variation curve with time. Through calculation, it can be seen that the relative error between the experimental and theoretical temperature is 9.58%, which is within the allowable tolerance within range.

Figure 11 shows the experimental measurement data at the 400-mm position of the ball screw and the theoretical simulation temperature change curve. Through calculation, it can be seen that the relative error between the experimental and theoretical temperature is 12.2%, which is within the allowable error within range.

In summary, the relative errors between the experimental data and theoretical simulation data at three locations at 100 mm, 200 mm, and 400 mm that we selected are all less than 15%, which is within the allowable range of error, verifying the theoretical model and solution results.

Table 2 The temperature of the screw shaft at different positions

Time/min	0 min	10 min	20 min	30 min	40 min	50 min
100 mm/℃	17.0	19.9	21.1	22.7	23.7	23.6
200 mm/℃	17.0	19.7	23.2	24.6	24.7	24.9
400 mm/℃	17.0	19.5	20.9	21.5	22.1	22.3

4 Influencing factors of BSFS

In this section, the nut is taken as the research object, and its influence on the temperature field change and thermal deformation of the system is studied by changing some basic parameters [39]. It can be found from Eq. (23) that the parameters that affect the temperature rise of the system include speed, initial preload, lead, and axial load.

4.1 The influence of rotational speed

As shown in Fig. 10, the temperature rise of the ball screw varies with the speed. Here, three different speeds of 1000 r/min, 2000 r/min, and 3000 r/min are selected to study the speed of the ball screw feed system and its temperature impact of the field. It can be seen that as the rotation speed increases, the temperature of the ball screw gradually increases. It can also be found that the faster the rotation speed, the shorter the time to reach thermal equilibrium. Therefore, when the machine is preheated, a higher speed is used for preheating, and the thermal equilibrium is reached faster to improve the processing accuracy.

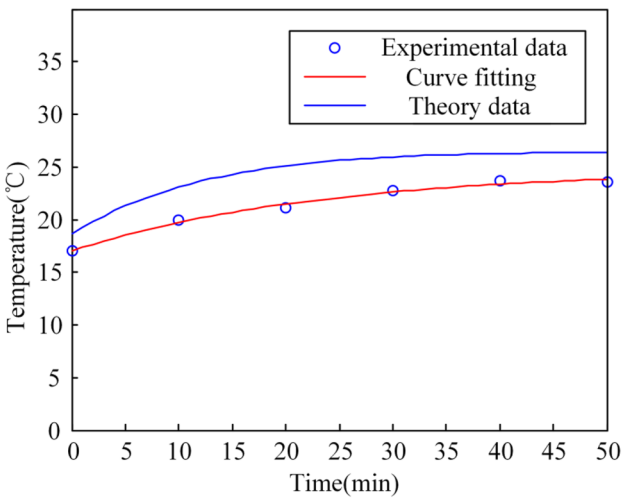

Fig. 9 Comparison of test and theoretical temperature of ball screw at 100 mm

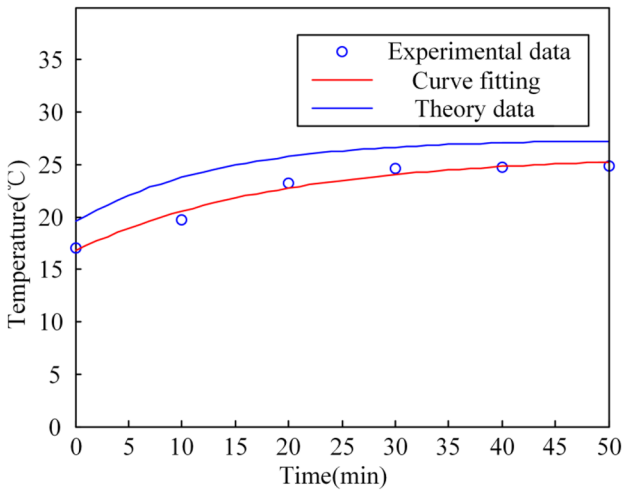

Fig. 10 Comparison of test and theoretical temperature of ball screw at 200 mm

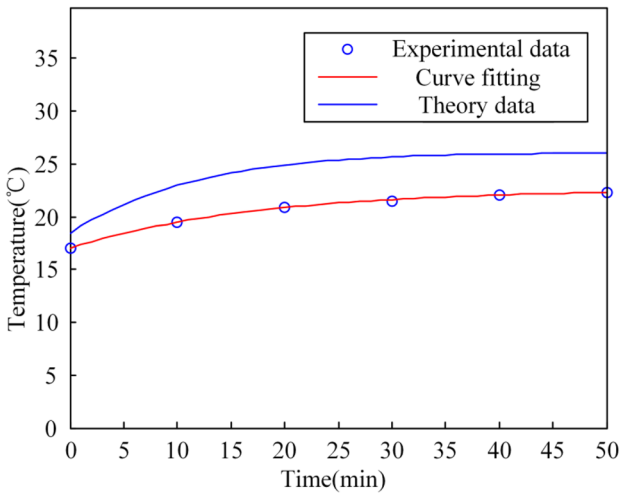

Fig. 11 Comparison of test and theoretical temperature of ball screw at 400 mm

In Fig. 12, the maximum temperature rise of the lead screw during thermal equilibrium can be obtained. According to the thermal deformation Eq. (26), the thermal deformation of the lead screw can be calculated as shown in Table 3. It can be found that as the temperature increases, the thermal deformation gradually becomes larger.

4.2 The influence of preload

Figure 13 shows the curve of the temperature rise of the ball screw with the initial preload. Three different initial preloads of 1000 N, 2000 N, and 3000 N are selected to study the preload of the ball screw feed system. The influence of its temperature field is as shown in Fig. 13. It can be seen that as the pre-tightening force increases, the temperature of the ball screw gradually increases.

Table 4 shows the maximum temperature and the thermal deformation of different preload. It can be found that as the temperature increases, the thermal deformation gradually becomes larger. The influence of preload on the temperature rise and thermal deformation of the ball screw is greater than the influence of the speed.

4.3 The influence of lead

Figure 14 shows that the lead of BSFS affects the temperature variation of the nut. Three different leads of 10 mm, 12 mm, and 15 mm are selected to study the lead of the ball screw feed system. As the lead of the ball screw increases, the temperature of the ball screw increases in general.

Table 5 shows the maximum temperature and thermal deformation of different lead. It can be found that as the temperature increases, the thermal deformation gradually becomes larger. There is an approximately linear increase between the change in temperature rise and thermal deformation and the lead.

4.4 The influence of Convection heat transfer coefficient

Figure 15 shows that the convection heat transfer coefficient of ball screw affects the temperature variation of the nut. Three different convection heat transfer coefficients of 100 W/(m^2·℃), 250 W/(m^2·℃), and 400 W/(m^2·℃) are selected to study the convection heat transfer coefficient of

Fig. 12 The temperature rising and thermal deformation of the lead screw changes with the speed

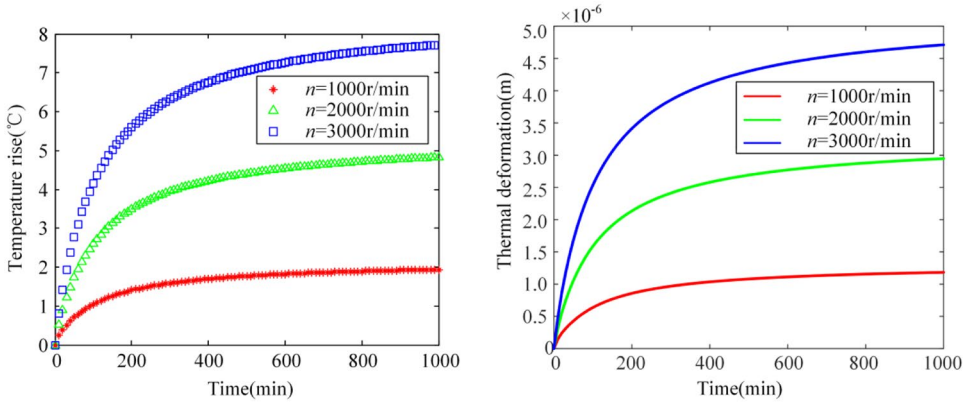

Table 3 Temperature rise and thermal deformation of the system at different speeds

Rotating speed (r/min)	Temperature rise (℃)	Thermal deformation (m)
1000	2.1	0.001178
2000	5.0	0.002939
3000	8.2	0.004698

Table 4 Temperature rise and thermal deformation of the system at different preload

Preload (N)	Temperature rise (℃)	Thermal deformation (m)
1000	3.3	0.001871
1500	4.7	0.002646
2000	5.9	0.003418

Table 5 Temperature rise and thermal deformation of the system at different preload

Lead (mm)	Temperature rise (℃)	Thermal deformation (m)
10	4.1	0.002147
12	5.1	0.002682
15	6.5	0.003485

Table 6 Temperature rise and thermal deformation of the system at different convection heat transfer coefficient

h_c (W/(m^2·℃))	Temperature rise (℃)	Thermal deformation (m)
100	10.4	0.006349
250	4.7	0.002890
400	3.1	0.001873

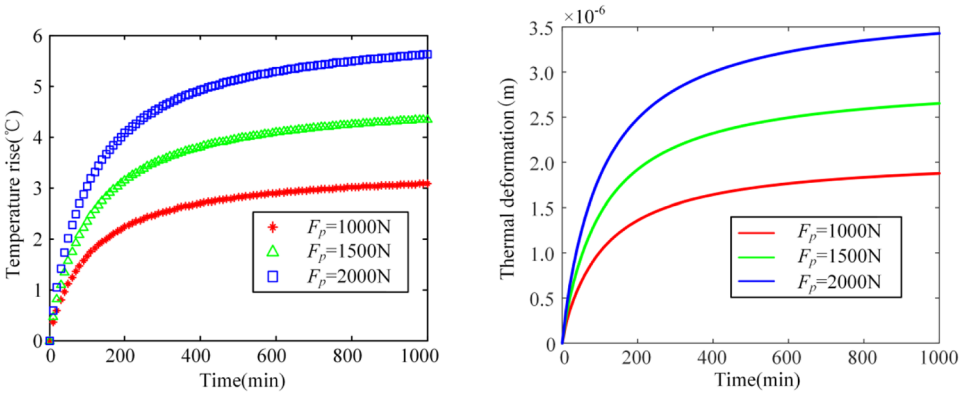

Fig. 13 The temperature rising and thermal deformation of the lead screw changes with the preload

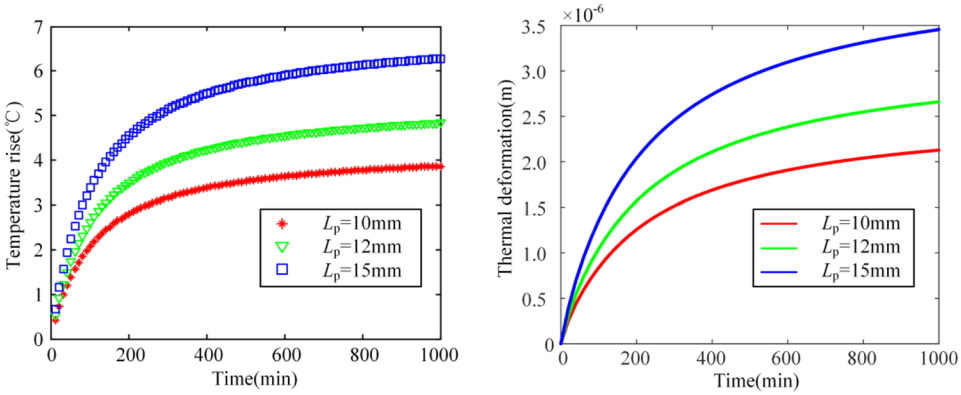

Fig. 14 The temperature rising and thermal deformation of the lead screw changes with the lead

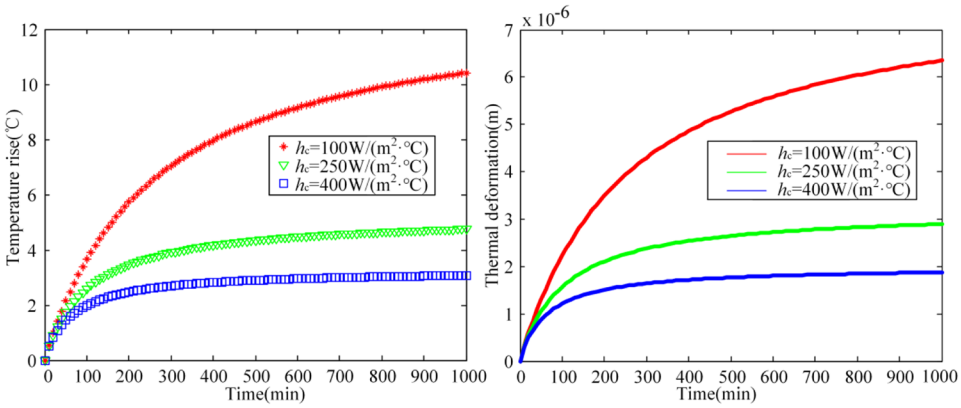

Fig. 15 The temperature rising and thermal deformation of the lead screw changes with the lead

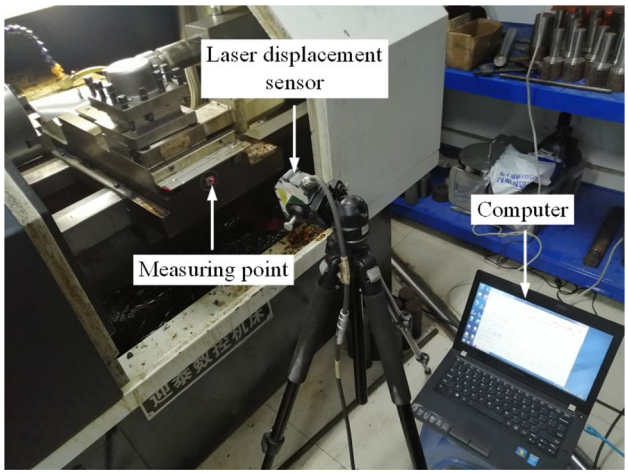

Fig. 16 Experimental site

Table 7 Comparison of test and theoretical value of influence of different rotation speed on thermal deformation of ball screw

Rotating speed (r/min)	Thermal deformation experiment (mm)	Thermal deformation Theoretical value (m)	relative errors
1000	0.001043	0.001178	11.46%
2000	0.002552	0.002939	13.16%
3000	0.004218	0.004698	10.21%

the ball screw feed system. As the convection heat transfer coefficient of the ball screw increases, the temperature of the ball screw reduces in general.

Table 8 Comparison of test and theoretical value of influence of different preload on thermal deformation of ball screw

Preload(N)	Thermal deformation experiment (mm)	Thermal deformation Theoretical value (m)	relative errors
1000	0.001650	0.001871	11.81%
1500	0.002312	0.002646	12.62%
2000	0.003015	0.003418	11.79%

Table 6 shows the maximum temperature and thermal deformation of different convection heat transfer coefficient. It can be found that as the temperature increases, the thermal deformation gradually becomes smaller. There is an approximately linear reduce between the change in temperature rise and thermal deformation and the lead. Therefore, in order to reduce the influence of thermal deformation, the convection heat transfer coefficient should be increased as much as possible.

4.5 Experimental verification

In order to further verify the correctness of the model, we experimented to record the axial thermal deformation of the ball screw at different speeds and preloads and recorded them. Because the nut has been installed and fixed, it will no longer be experimentally verified. As shown in Fig. 16, we use the laser displacement sensor to measure the deformation of the end of the ball screw and recorded the data in Tables 7 and 8.

Through calculation, it can be found that the relative errors between the experimental measured value and the theoretical calculated value of the thermal deformation of the ball screw at different speeds and different preloads are within the allowable error within range; this shows that our simulation is reliable.

5 Conclusion

This paper solves the thermal error model of the ball screw by using the Fourier series expansion method and investigates the relationship between the temperature rise and thermal deformation of the ball screw. We got the temperature field model of the BSFS. Based on the results and analysis, some conclusions can be drawn as follows:

1. As time increases, the temperature of the lead screw gradually rises and finally reaches a thermal equilibrium state; as the length of the lead screw increases, the thermal elongation of the axis will increase.
2. As the speed, preload and lead increase, the temperature and thermal deformation of the ball screw gradually increase. The influence of preload on the temperature rising and thermal deformation of the ball screw is greater than the influence of the speed on it.

Author contribution Jiancheng Yang: methodology; investigation; experimental; writing-original draft; writing-review and editing. Changyou Li: resources and supervision. Mengtao Xu: resources, writing-reviewing and editing, supervision, writing-review and editing. Yimin Zhang: resources and supervision.

Funding The work was supported by National Natural Science Foundation of China (Grant No. 52075087), the Fundamental Research Funds for the Central Universities (Grant No. N2003006 and N2103003), and National Natural Science Foundation of China (Grant No. U1708254).

Availability of data and material The data sets supporting the results of this article are included within the article and its additional files.

Declarations

Ethics approval This chapter does not contain any studies with human participants or animals performed by any of the authors.

Consent to participate Not applicable. The article involves no studies on humans.

Consent for publication All authors have read and agreed to the published version of the manuscript.

Conflict of interest The authors declare no competing interests.

References

1. Hu S, Ma C, Y J, Zhao L, Mei X, Gong G (2015) Investigation into effect of thermal expansion on thermally induced error of ball screw feed drive system of precision machine tools. Int J Mach Tools Manuf 9760–17
2. Mayr J, Jedrzejewski J, Uhlmann E (2012) Thermal issues in machine tools. CIRP Ann Manuf Technol 61(2):771–791
3. Venugopal R, Barash M (1986) Thermal effects on the accuracy of numerically controlled machine tools. CRIP Ann Manuf Techn 35(1):255–258
4. Week M, Zangs L (1975) Computing the thermal behavior of machine tools using the finite element method-possibilities and limitations. Proc 16th MTDR Confe 16:185–194
5. Xu ZZ, Liu XJ, Kim HK, Shin JH, Lyu SK (2011) Thermal error forecast and performance evaluation for an air-cooling ball screw system. Int J Adv Manuf Tech 51(7–8):605–611
6. Ming X, Jiang S (2011) A thermal model of a ball screw feed drive system for a machine tool. Proc Inst Mech Eng Part C J Mech Eng Sci 225(1):186–193
7. Li Z, Fan K, Yang J, Zhang Y (2014) Time-varying positioning error modeling and compensation for ball screw systems based on simulation and experimental analysis. Int J Adv Manuf Tech 73:5–8
8. Oyanguren A, Larrañaga J, Ulacia I (2018) Thermo-mechanical modelling of ball screw preload force variation in different working conditions. Int J Adv Manuf Technol 2:1–17
9. Huang S, Feng P, Xu C, Ma Y, Ye J, Zhou K (2018) Utilization of heat quantity to model thermal errors of machine tool spindle. Int J Adv Manuf Tech 97(5_8):1733–1743
10. Li T, Zhao C, Zhang Y (2017) Adaptive real-time model on thermal error of ball screw feed drive systems of CNC machine tools. Springer, London 94(9–12):3853–3861
11. Yun WS, Kim SK, Cho DW (1999) Thermal error analysis for a CNC lathe feed drive system. Int J Mach Tools Manuf 39:1087–1101
12. Ramesh R, Mannan MA, Po AN (2003) Thermal error measurement and modeling in machine tools. Part I Influence of varying operation condition, Int J Mach Tools Manuf 43:391–440
13. Xu ZZ, Liu XJ (2011) Thermal error forecast and performance evaluation for an air-cooling ball screw system. Int J Mach Tools Manuf 51:605–611
14. Xu ZZ, Liu XJ (2014) Study on thermal behavior analysis of nut/shaft air cooling ball screw for high-precision feed drive. Int J Precis Eng Manuf 15:123–128
15. Zhang Y, Yang JG, Jiang H (2012) Machine tool thermal error modeling and prediction by grey Neural network. Int J Adv Manuf Technol 59(9–12):1065–1072
16. Lee J, Lee JH, Yang SH (2001) Thermal error modeling of a horizontal machining center using fuzzy logic strategy. J Manuf Process 3(2):120–127
17. Ma C, Yang J, Mei XS, Zhao L, Dong HS, Zhang S (2017) Dynamic thermal-structure coupling analysis and experimental study on ball screw feed drive system of precision machine tools. Appl Mech Mater 868:124–135
18. Han J, Wang LP, Wang HT (2012) A new thermal error modeling method for NC machine tools. Int J Adv Manuf Technol 62:205–212
19. Wu CW, Tang CH, Chang CF, Shiao YS (2012) Thermal error compensation method for machine center. Int J Adv Manuf Technol 59:681–689
20. Wang W, Zhang Y, Yang JG, Zhang YS, Yuan F (2012) Geometric and thermal error compensation for CNC milling machines based on Newton interpolation method. Proc IME C J Mech Eng Sci 227:771–778
21. Wu H, Zhang HT, Guo QJ, Wang XH, Yang JG (2008) Thermal error optimization modeling and real-time compensation on a CNC turning center. J Mater Process Tech 207:172–179
22. Xu ZZ, Choi C, Liang LJ (2015) Study on a novel thermal error compensation system for high-precision ball screw feed drive (1st report: model, calculation and simu- lation). Int J Precis Eng Man 16:2005–2011
23. Xu ZZ, Choi C, Liang LJ (2015) Study on a novel thermal error compensation system for high-precision ball screw feed drive (2nd report: experimental verification). Int J Precis Eng Man 16:2139–2145
24. Zhang J, Li B, Zhou C, Zhao W (2016) Positioning error prediction and compensation of ball screw feed drive system with different mounting conditions. Proc Inst Mech Eng Part B J Eng Manuf 230(12)
25. Wei X, Gao F, Li Y, Zhang D (2018) Study on optimal independent variables for the thermal error model of CNC machine tools. Int J Adv Manuf Tech 98:(1–4)
26. Sun YP, Wang DL, Dong HM (2016) A seven-sensor con- figuration method for testing thermal error of a horizontal machining center

with linear optical grating scale. Proc IMechE, Part C: J Mech Eng Sci 231:2681–2689
27. Li Y, Zhang J, Su D, Zhou C, Zhao W (2018) Experiment-based thermal behavior research about the feed drive system with linear scale. Adv Mech Eng 10(11):168781401881235
28. Harris TA (1991) Rolling Bearing Analysis. Wiley & Sons, New York
29. Tian R, He R (2004) Solution for heating of ball screw and environmental engineering, World Manuf. Eng Mark 3:65–67
30. Verl A, Frey S (2010) Correlation between feed velocity and preloading in ball screw drives. Ann CIRP 59(2):429–432
31. Xu ZZ, Liu XJ, Kim HK, Shin JH, Lyu SK (2011) Thermal error forecast and performance evaluation for an air-cooling ball screw system. Int J Mach Tools Manuf 51:605–611
32. Xia J, Hu Y, Wu B, Shi T (2009) Research on thermal dynamics characteristics and modeling approach of ball screw. Int J Adv Manuf Tech 43:(5–6)
33. Hu S, Ma C, Y J, Zhao L, Mei X, Gong G, (2015) Investigation into effect of thermal expansion on thermally induced error of ball screw feed drive system of precision machine tools. Int J Mach Tools Manuf 97:60–17
34. Liu B (2013) Research on temperature field and thermal deformation of feed system of gantry machining center. Nanjing Univ Aeronaut Astronaut
35. Bapat VA, Srinivasan P (1971) Method of separation of variables for the solution of certain nonlinear partial differential equations. J Eng Mech 93(2):162
36. Zhang D, Jia H (2007) Numerical analysis of leaky modes in two-dimensional photonic crystal waveguides using Fourier series expansion method with perfectly matched layer E90C(3):613–622
37. Yuan J, Yang J, Jun N (1999) Thermal error mode analysis and robust modeling for error compensation on a CNC turning center. Int J Mach Tools Manuf 39(9):1367–1381
38. Zhang LC, Zu L (2019) A new method to calculate the friction coefficient of ball screws based on the thermal equilibrium. Adv Mech Eng 11(1):168781401882073
39. Li R, Lin W, Zhang J, Chen Z, Li C, Shuang Q (2018) Research on thermal deformation of feed system for high-speed vertical machining center. Procedia Comput Sci 131:469–476